Quaternary International xxx (xxxx) xxx

Contents lists available at ScienceDirect

Quaternary International

journal homepage: www.elsevier.com/locate/quaint

Revised OSL chronology of the Kisiljevo loess-palaeosol sequence: New insight into the dust flux in the eastern Carpathian Basin during MIS 3 - MIS1

Zoran M. Perić [a,*], Cathal Ryan [b], Helena Alexanderson [a], Slobodan B. Marković [c,d,e]

[a] Department of Geology, Lund University, Sölvegatan 12, SE-223 62, Lund, Sweden
[b] Irish Climate Analysis and Research Units, Department of Geography, Maynooth University, Maynooth, Ireland
[c] LAPER – Laboratory for Environmental reconstruction, Faculty of Science and Mathematics, University of Novi Sad, Trg Dositeja Obradovića 3, 21000 Novi Sad, Serbia
[d] Serbian Academy of Sciences and Arts. Knez Mihajlova 35, 11000, Belgrade, Serbia
[e] University of Montenegro. Cetinjska 2, 81000, Podgorica, Montenegro

ARTICLE INFO

Keywords:
Optically stimulated luminescence
Quartz
Age models
Revised chronology
Loess

ABSTRACT

This study presents a detailed investigation of the Kisiljevo loess-palaeosol sequence in north-eastern Serbia, offering a refined understanding of its paleoenvironmental dynamics. Contrasting our updated OSL chronology with a previous study, reveals discrepancies, particularly at 400 cm depth, where a considerable age underestimation is evident. While variations in sampling depth and methodology may contribute to some differences, the substantial deviation raises concern about the reliability of the earlier chronology. Our robust age-depth model constructed using Bayesian modelling, and the consistent increase in ages with depth suggest a potential underestimation in the uppermost layer of the earlier study, possibly due to partial bleaching or post-depositional mixing. The Bayesian age-depth model portrays a continuous sedimentation history from the later stages of Marine Isotope Stage 3 (MIS 3) to the present day. The patterns in the calculated Mass Accumulation Rates reveal distinctive peaks during MIS 3 and the middle of MIS 2, deviating from typical dust deposition models. The MIS 3 peaks in dustiness could be attributed to regional factors such as increased transportation rates, enhanced trapping efficiency, or elevated palaeowind intensity. This research not only enhances our understanding of the Kisiljevo LPS but also provides valuable insights into regional paleoenvironmental dynamics. The study emphasizes the importance of considering local geological variations in reconstructing past climates from sediment archives and sets the stage for further investigations into the factors influencing dust deposition in north-eastern Serbia. The MAR trends established here serve as a crucial reference for broader paleoclimatic interpretations in the Carpathian Basin.

1. Introduction

One of the most fundamental requirements for an accurate reconstruction of the palaeoclimates from sediment archives (loess in this case) are reliable and independent absolute chronologies. In this context, during the last few decades, optically stimulated luminescence dating (OSL) established itself as one of the most utilized geochronological methods. One of the main reasons is that, contrary to other dating methods, OSL determines the time of the sediment deposition. Considering the predominant aeolian origin of loess, it is highly probable that the luminescence signal underwent complete resetting before deposition. This is a crucial prerequisite for luminescence dating, rendering loess deposits particularly well-suited for the application of luminescence techniques (Wintle, 1993, p. 199). The first OSL chronology for the Kisiljevo LPS was reported by Perić et al. (2022a). In that study, only four quartz OSL ages were presented, for the lower 4 m of the profile and in a lower resolution. While, not always the case, OSL chronologies constructed with only few ages are often prone to errors and/or misinterpretations, especially when there are no overlying (or underlying) samples which could provide a certain degree of age control. Here we present an updated, high resolution OSL chronology for the Kisiljevo loess-palaeosol sequence (LPS) in north-eastern Serbia, using 63–90 μm quartz. We provide details about the conducted measurements, analytical procedures and characteristics of the observed OSL signals. Since

* Corresponding author.
E-mail address: zoran.peric@geol.lu.se (Z.M. Perić).

https://doi.org/10.1016/j.quaint.2024.06.006
Received 8 April 2024; Received in revised form 10 June 2024; Accepted 12 June 2024

any inaccuracies in constructed OSL chronologies ultimately result in erroneous dust mass accumulation rate (MAR) calculations, here we constructed a new and improved age model using the rbacon age-depth modelling software (Blaauw and Christen, 2011). Subsequently, we apply the age model to reconstruct changes in MARs. To the best of our knowledge this study presents the most detailed luminescence-based chronology for a LPS in north-eastern Serbia.

2. Regional setting and site description

The Kisiljevo LPS is located on the eastern outskirts of the homonymous village, situated at coordinates 44°44′0″ N and 21°25′0″ E, on the southern shores of a former Danube River channel (so called Srebrno Jezero artificial lake), approximately 29 km northeast of Požarevac city (Fig. 1). Positioned at an elevation of 69 m above mean sea level, the site extents in an east-west direction. Kisiljevo is situated in undulating lowlands, surrounded by low mountain ranges to the south.

During the initial investigations, it was assumed that the Kisiljevo LPS is a small, isolated loess "spot" that may have been more extensive in the past but has been reduced to its current dimensions due to fluvial erosion (Perić et al., 2022a). However, upon a more detailed field survey, it was found that the investigated profile presents only a small, exposed section at the east most side of a (presumably) much larger loess plateau. Such a geomorphological setting is relatively stable and is therefore more likely to preserve a more continuous accumulation record (without sedimentary hiatuses) and be less susceptible to post-depositional reworking (Frechen et al., 2003).

Although, the area is either covered by dense vegetation or agricultural surfaces (most of which is private property) which made a more detailed investigation not viable, it was possible to conclude some general characteristics of the loess coverage, based on observations and field interpretations (following and detecting the loess horizon). The loess covered area extends ~2 km west of the investigated opened profile at Kisiljevo and at least another ~0.5 km south (Fig. S1). The northern side of the site, covered with dense forest and bush vegetation, shows a distinct loess horizon extending ~2 km in the north-west direction. In at least two gullies the loess horizon is exposed at the top, where the visible thickness reaches more than 5 m (Fig. S2 and Fig. S3). At the furthest (visible) west boundary of the site, the thickness decreases, the loess horizon is less noticeable and farming surfaces gradually become dominant. To the south, the loess profile is traversed by a road connecting Kisiljevo to the nearby settlements of Ram and Biskuplje, dividing the loess exposure into two sections. The south section is far less pronounced than the north one investigated in this study, reaching only ~2 m of thickness. Unfortunately, at present, it is not possible to determine the true extent of the loess covered area. Most of the surface south of the road was completely transformed into farming land and to the west it is covered by dense forest vegetation, which makes detailed surveys problematic.

The examination of the geological profile involved a detailed analysis of the vertical loess cliff through in situ observations, as illustrated in Fig. 2. Previous investigations of the Kisiljevo LPS, determined the thickness of the section at ~8 m. However, during the field investigations and sampling, we were able to reveal another meter of loess sediment at the base, which sets the thickness of the Kisiljevo LPS at ~9 m.

In the vicinity of Kisiljevo, the prevailing Holocene soil is usually of

Fig. 2. The Kisiljevo LPS showing: A. the initial sampling surface by Perić et al. (2022a), and B. The surface sampled for this study.

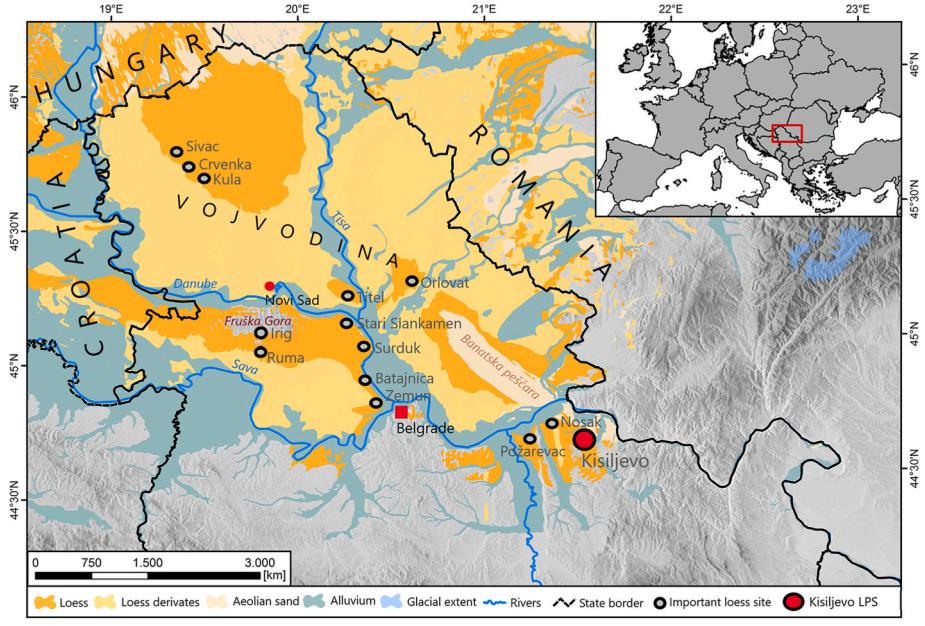

Fig. 1. Map of loess distribution in the Vojvodina region and north-eastern Serbia, showing the geographical position of the Kisiljevo LPS and other key loess sites referred to in text. Distribution of loess, loess derivates, aeolian sand and alluvium is shown according to Lehmkuhl et al. (2018). Modified from Perić et al. (2022a).

chernozem characteristics. The recent soil layer (S0) at the sampling site, measures ~50 cm in thickness and is comprised of a Ck horizon containing abundant $CaCO_3$ nodules ranging from 1 to 5 cm in diameter. Additionally, numerous crotovinas and root channels containing humic material are present. The transitional AC horizon, spanning 20 cm, exhibits a porous nature with a silty loam texture and a granular structure. The subsequent silty loam Ah horizon, with a thickness ranging from 40 to 60 cm, features a granular structure and includes carbonate pseudomycelia (Perić et al., 2022a, Fig. 3). Beneath these layers lies the loess unit (L1), extending ~820 cm in depth and characterized by a light yellow to grey colour. This layer is coarse, porous, and massive, lacking visible signs of soil development. At the interface with the Holocene soil (S0), spherical soft carbonate nodules and humic infiltrations within old root channels are discernible. During previous investigations of the profile, it was noted that, at a depth of approximately 7 m, a distinct layer, potentially a tephra, is interbedded with the loess, measuring around 50 cm in thickness (Perić et al., 2022a). However, after a conducted geochemical analysis, this assumption could not be confirmed. Moreover, during the recent field survey, this layer was not detectible. It is more likely that this darker layer presented a weakly developed palaeosol which was masked due to weathering. It is also possible that the vicinity of the Danube alluvial plain may have caused sudden changes in the deposition of local layers of different granularity which was subsequently misinterpreted as a tephra layer.

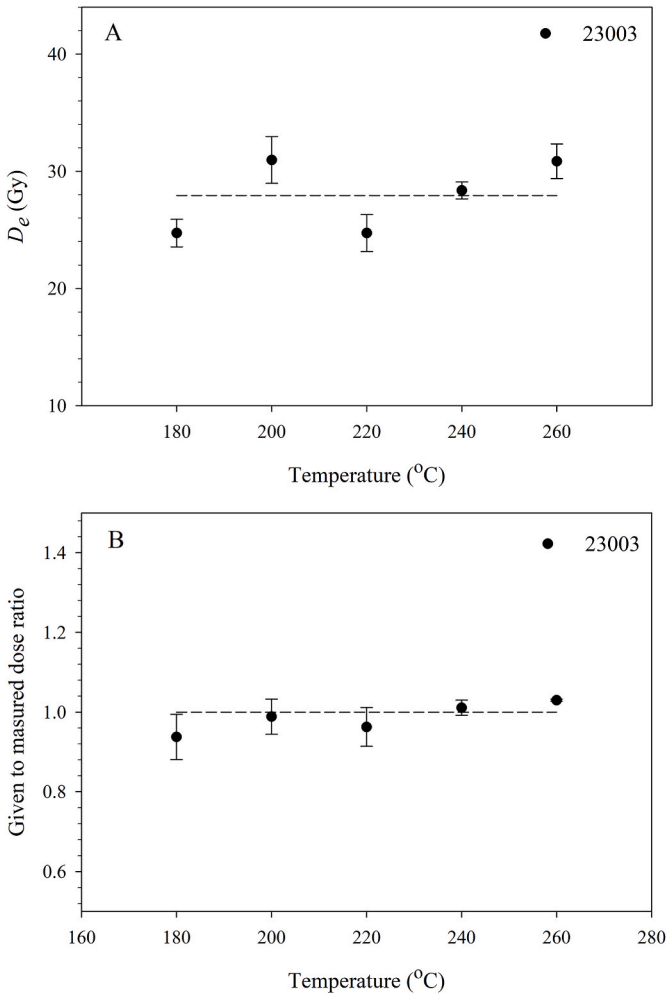

Fig. 3. A. Preheat plateau results for sample 23003. The error bars represent one standard error. The dashed line is drawn on the mean D_e value calculated from all five temperature points. B) Preheat plateau/dose recovery test results for sample 23003. The dashed line is drawn at the ideal 1:1 dose recovery ratio.

3. Methods

3.1. Sample preparation and facilities

Compared to the strategy presented in the previous study (Perić et al., 2022a), the sampling for luminescence dating was conducted ~10 m to the west (Fig. 2), thus avoiding the eroded and collapsed overhang part of the section.

The luminescence dating samples were recovered by hammering stainless steel tubes (20 cm length, 5 cm diameter) into the freshly cleaned profile. A total of 19 samples were gathered, in a 50 cm resolution, ranging from 10 cm to 900 cm depth. The luminescence samples underwent processing in the Lund luminescence laboratory, Lund University, Sweden under low-intensity red light conditions. The inner material of the cylinders was utilized for equivalent dose (D_e) measurements, while the outer material (approximately 2 cm), likely exposed to sunlight, was used for determining water content and dose rates.

For D_e measurements, the extracted sediment underwent wet sieving through 90, 63, and 40 μm sieves. Because of its abundance, and the experience from previous studies on OSL dating of Serbian loess (e.g. Perić et al., 2019, 2022a), the 63–90 μm material was chosen for sample preparation. The 63–90 μm sediment was treated with 10% HCL (60 min) and 10% H_2O_2 (60 min) to eliminate carbonates and organic matter, respectively. To isolate the quartz fraction, the material was submerged in sodium heteropolytungstate dissolved in water (2.62 g cm^{-3}; LST 'Fastfloat') for 24 h. The >2.62 g cm^{-3} quartz fraction was then treated with a 40% HF solution for 90 min to remove any remaining feldspar contamination. Subsequently, a 10% HCL treatment for 120 min was applied to remove fluorides. After each treatment step, the samples underwent three washes with deionized water. All samples yielded sufficient quartz grains for reliable D_e measurements. The quartz grains were mounted as large 8 mm aliquots on stainless steel discs using silicone oil spray as an adhesive. Luminescence measurements were conducted using Risø TL/OSL DA-20 readers (Bøtter-Jensen et al., 2003) equipped with blue LEDs (470 nm, ~80 mW cm^{-2}) and infrared (IR) LEDs (870 nm, ~135 mW cm^{-2}). Irradiation was carried out using a $^{90}Sr/^{90}Y$ beta source calibrated using the Risø calibration quartz, batch 123 (Hansen et al., 2015). Quartz OSL signals were collected through 7.5 mm of Schott U-340 (UV) glass filter.

3.2. Dose rate measurements

The sediment dose rate was measured using the μDose system, at the Lund luminescence laboratory, as described by Kolb et al. (2022) and Tudyka et al. (2023). Initially, the material underwent a drying process at 105 °C for a duration of 24 h, following which approximately 20 g of the sediment were finely ground to a size <20 μm. Subsequently, precisely 3 g of the dried and ground sample were placed in a 70 mm diameter holder. Finally, the concentrations of ^{238}U, ^{232}Th and ^{40}K were determined by analysing the samples for >24 h.

The dry dose rates for the radionuclides in the quartz were determined by applying the conversion factors presented by Guérin et al. (2011). The water content of the sediment was determined directly for each collected sample. However, in most cases, the calculated water content displayed very low values and ranged from 4% for sample 23001 to 1% for samples 23005–23018. The observed low values could be attributed to prolonged exposure of the Kisiljevo section to air before sampling, as it is often the case for LPS in this region.

Consequently, we deem the measured water content as unreliable estimates over geological time. Hence, relying on the topographic and geologic context for the site, along with insights from prior studies (e.g. Antoine et al., 2009; Perić et al., 2022a, 2022b; 2021; Schmidt et al., 2010) the water content was approximated to be 12 ± 5%, assuming this value remained constant throughout the burial period. The alpha and beta attenuation factors were estimated using the calculations of

Brennan et al. (1991) and Guérin et al. (2012) respectively, and dose rate conversion factors were obtained from Guérin et al. (2011). The contribution of cosmic radiation was taken into account and calculated based on the methodology outlined by Prescott and Hutton (1994). This calculation was performed for each sample, factoring in depth, altitude, and geomagnetic latitude, with an assumed uncertainty of 10%.

3.3. D_e measurements

Equivalent doses were determined employing the Single Aliquot Regenerative Dose (SAR) protocol, following the procedures of Murray and Wintle (2003, 2000). The quartz grains underwent measurements with preheat and cut-heat temperatures set at 240 °C and 200 °C, respectively. The choice of the preheat and cut-heat temperatures is discussed below. Optical stimulation was conducted for 40 s at 125 °C using blue LEDs. The relevant luminescence signal for analysis was integrated over the initial 0.16 s of the decay curve, with an early background (0.32–0.48 s interval) subtracted from the net signal. Sensitivity changes were corrected using the OSL signal to a test dose (10% of the assumed natural dose was applied in all measurements). Post each SAR cycle, a high-temperature bleach at 280 °C was conducted for 40 s, following the protocol by Murray and Wintle (2003). Intrinsic tests, including recycling and recuperation, were incorporated into each measurement as outlined in the SAR protocol (Murray and Wintle, 2003). The purity of quartz grains was assessed through the IR depletion test (Duller, 2003). A tolerance of a 10% deviation from unity was applied for recycling and IR depletion tests. For the recuperation signal, a value of 5% of the natural signal was deemed acceptable. The aliquots that did not meet these requirements (1%) were rejected and not used for the D_e calculations. The outliers were identified using the interquartile range (1.5 x IQR) and were not used in the D_e calculations (~2% of the measured aliquots). All the luminescence data were analysed using the Risø Analyst software, version 4.57 (Duller, 2015). The calculated D_es for each sample present the weighted means of the individual D_es. The age calculation was conducted using the DRAC Dose Rate and Age Calculator v. 1.2 (Durcan et al., 2015). The calculated D_es, OSL ages, and dose rates are presented in Table 1.

3.4. Age-depth modelling

The calculated OSL ages enabled us to construct an improved, continuous, and fully independent age versus depth model for the Kisiljevo LPS, over the investigated time period. Here we apply the Bayesian modelling method using the rbacon code by Blaauw and Christen (2011). The section thickness was set to 20 cm and the resolution of the subdivisions along the sediment profile to 5 cm.

To ensure consistent comparability across various regions and other repositories of dust, and to facilitate the estimation of past atmospheric dust flux (Albani et al., 2015), we have additionally calculated the Mass Accumulation Rate (MAR) (Kohfeld and Harrison, 2003), using the rbacon age-depth modelling results. The MARs were calculated using the equation:

$$\mathrm{MAR} = \mathrm{SR} \times \mathrm{BD} \times f_{\mathrm{eol}}$$

where SR represents the sedimentation rate (m/a), BD is the dry bulk density and f_{eol} is the fraction of aeolian sediment (Kohfeld and Harrison, 2001). Here, we presume that the source of the loess is entirely aeolian, and therefore, we assign a value of 1.

In this study, direct measurements of BD were not conducted. Instead, estimates from other sections of the middle Danube, providing average values of 1.5 g cm^{-3}, were utilized (Újvári et al., 2010). The MAR values in this study are given without uncertainty estimates. Currently, there is no agreeable method to derive accurate uncertainty estimates for dust MAR from loess deposits (e.g. Perić et al., 2022b, 2020; Stevens et al., 2011; Újvári et al., 2010). Beyond potential uncertainties in bulk density estimates and the influence of post-depositional alteration, the application of simple Gaussian error propagation from luminescence ages might not be appropriate, as the uncertainty may not strictly follow a Gaussian distribution or be entirely random. Despite these challenges, it is posited that the absolute MAR estimates are proportionally more uncertain when compared to the luminescence ages (Perić et al., 2022b).

4. Results

4.1. Preheat plateau and dose recovery tests

To establish suitable preheat conditions for the SAR protocol, we conducted a preheat plateau test on 18 aliquots from sample 23003 (Murray and Wintle, 2000). During the initial preheat, temperatures ranging from 180 to 260 °C (in 20 °C increments; three aliquots per temperature point) were applied for a duration of 10 s. The cut–heat temperatures for the test dose preheat were consistently maintained 40 °C lower than the preheat temperatures. The D_e value did not show any significant sensitivity to preheat temperature up to approximately 260 °C. The recycling ratios are close to unity and the recuperation is close to 1% over the 180–260 °C first preheat period.

A discernible plateau could not be observed in the of 180–260 °C

Table 1
Summary of depth information, sample codes, radionuclide concentrations, total dose rates, weighted average D_e values, OSL ages and total errors in ka for the Kisiljevo LPS. n represents the number of aliquots. Error terms are given as 1 standard error of the mean.

Depth (cm)	Sample ID	K (%)	Th (ppm)	U (ppm)	OSL dose rate (Gy ka $^{-1}$)	n	OSL D_e (Gy)	OSL age (ka)
10	23001	1.67 ± 0.06	11.23 ± 0.86	3.21 ± 0.26	3.21 ± 0.14	23	1.47 ± 0.13	0.46 ± 0.04
50	23002	1.43 ± 0.07	11.18 ± 1.52	3.78 ± 0.46	3.06 ± 0.16	24	20.40 ± 1.07	6.66 ± 0.49
100	23003	1.25 ± 0.07	9.08 ± 1.36	3.03 ± 0.41	2.57 ± 0.14	24	34.72 ± 1.93	13.50 ± 1.04
150	23004	1.22 ± 0.07	10.73 ± 1.31	2.57 ± 0.39	2.54 ± 0.13	24	48.83 ± 1.86	19.22 ± 1.25
200	23005	1.24 ± 0.06	10.16 ± 0.73	2.61 ± 0.22	2.52 ± 0.11	24	51.58 ± 2.14	20.51 ± 1.24
250	23006	1.24 ± 0.07	9.16 ± 1.44	3.04 ± 0.43	2.54 ± 0.14	28	50.77 ± 1.49	19.97 ± 1.25
300	23007	1.29 ± 0.07	12.43 ± 1.38	2.48 ± 0.41	2.67 ± 0.14	24	51.85 ± 1.25	19.45 ± 1.12
350	23008	1.24 ± 0.07	10.92 ± 1.48	2.81 ± 0.44	2.59 ± 0.14	24	63.76 ± 2.12	24.64 ± 1.59
400	23009	1.28 ± 0.07	12.61 ± 1.39	2.03 ± 0.41	2.56 ± 0.14	23	66.79 ± 1.98	26.11 ± 1.61
450	23010	1.30 ± 0.06	10.11 ± 0.90	3.14 ± 0.27	2.65 ± 0.12	22	71.42 ± 2.04	26.92 ± 1.46
500	23011	1.20 ± 0.07	7.67 ± 1.44	3.74 ± 0.44	2.53 ± 0.14	24	81.90 ± 3.82	32.37 ± 2.36
550	23012	1.29 ± 0.07	9.73 ± 1.40	3.45 ± 0.42	2.67 ± 0.14	23	91.74 ± 3.35	34.40 ± 2.23
600	23013	1.19 ± 0.06	12.37 ± 1.19	3.34 ± 0.36	2.73 ± 0.14	23	79.39 ± 2.66	29.10 ± 1.74
650	23014	1.30 ± 0.06	11.16 ± 0.83	3.08 ± 0.25	2.69 ± 0.12	23	95.25 ± 4.02	35.45 ± 2.19
700	23015	1.36 ± 0.07	13.46 ± 1.45	2.33 ± 0.43	2.72 ± 0.15	22	98.14 ± 4.09	36.15 ± 2.46
750	23016	1.32 ± 0.07	9.43 ± 1.58	3.80 ± 0.48	2.73 ± 0.15	20	101.31 ± 4.88	37.05 ± 2.74
800	23017	1.19 ± 0.07	10.32 ± 1.51	3.12 ± 0.46	2.52 ± 0.15	24	83.18 ± 4.44	32.99 ± 2.59
850	23018	1.16 ± 0.06	8.89 ± 0.61	2.40 ± 0.18	2.25 ± 0.10	23	82.77 ± 3.74	36.87 ± 2.34
900	23019	1.36 ± 0.06	11.14 ± 0.98	2.85 ± 0.29	2.67 ± 0.13	23	91.62 ± 2.81	34.36 ± 1.96

temperature range, where all the measured D_e values exhibited scattering (Fig. 3A). Hence, we conducted a preheat plateau/dose recovery test on 18 bleached aliquots of sample 23003 in the same manner as for the preheat plateau test. Initial bleaching of natural aliquots was carried out using blue LEDs at room temperature for a duration of 100 s, followed by a pause of 10,000 s. After the pause, additional bleaching was performed at room temperature for 100 s (Murray and Wintle, 2003). Following this, a laboratory β-dose was applied to the previously bleached aliquots, matching the assumed natural D_e (~25 Gy), and was measured using a SAR protocol (Murray and Wintle, 2000). The protocol involved variations in the preheat temperature within the range of 180–260 °C, with the cut-heat temperature set 40 °C lower. The test dose was set at 20% of the given dose (~5 Gy) The results of the test are presented in Fig. 3B. The dose recovery ratio varied between 0.94 ± 0.06 for the 180 °C to 1.03 ± 0.00 for the 260 °C preheat temperature. A small plateau was observed between 240 and 260 °C. Consequently, based on these findings, we adopted a first preheat temperature of 240 °C for 10 s and a cut heat of 200 °C for all quartz measurements in this study.

To assess the effectiveness of the chosen SAR protocol, a dose recovery test (Murray and Wintle, 2003) was conducted on samples 23005, 23009, 23014 and 23019 (six aliquots per sample). These aliquots underwent two bleaching sessions using blue LEDs, each lasting 250 s at room temperature. A pause of 10,000 s was introduced between the two bleaching treatments. Subsequently, the aliquots were exposed to beta doses of approximately 40 (sample 23005), 60 (sample 23009), 80 (sample 23014), and 110 Gy (sample 23019). The measurement was conducted in the same manner as for the preheat plateau/dose recovery test. The results of the test are shown in Fig. 4. The measured to given dose ratio ranged from 1.03 ± 0.05 for sample 23005 to 1.04 ± 0.06 for sample 23019. It can be seen that the chosen SAR protocol is able to accurately measure doses of up to at least 110 Gy administered before any thermal pre-treatment.

4.2. Quartz OSL properties and D_e

A representative dose response (DRC) and decay curve (inset) for sample 23005 are shown in Fig. 5. The dose response curves were best fitted using a single saturating exponential or an exponential + linear function. The optically stimulated luminescence (OSL) signal induced by blue light shows a rapid decay during the first second of stimulation,

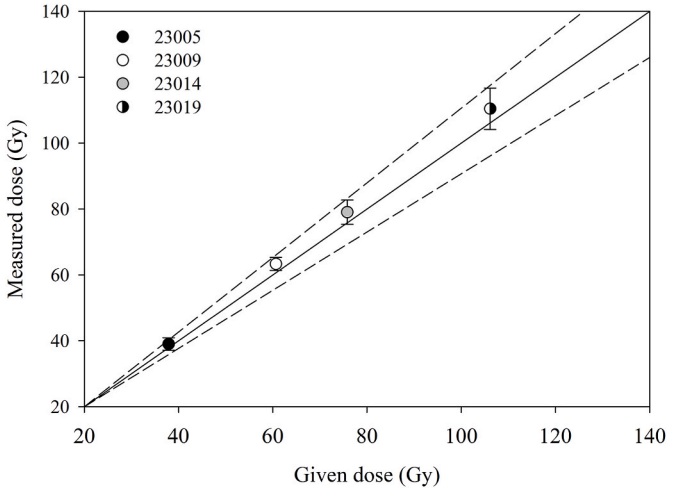

Fig. 4. Dose recovery results for four of the Kisiljevo samples. The given irradiation doses were chosen to match as closely as possible the likely equivalent dose of each sample. The test doses were set at ~20% of the given dose. Three aliquots were measured per sample. The calculated D_es present the weighted means of the individual D_es. The solid line indicates the ideal 1:1 dose recovery ratio while the dashed lines represent 10% deviation from unity.

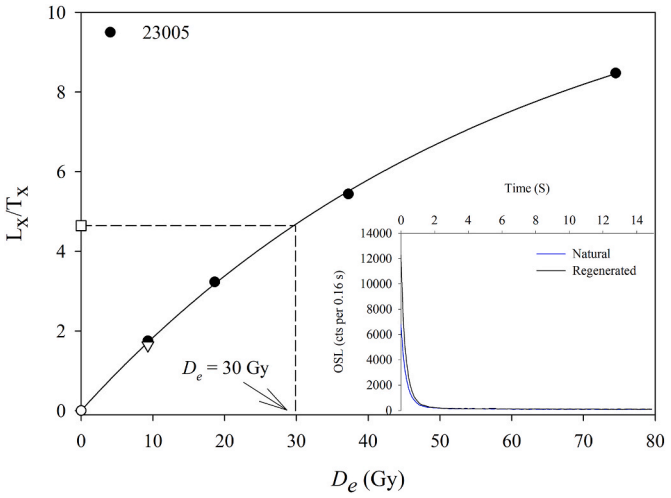

Fig. 5. Representative sensitivity-corrected luminescence dose response curve for one aliquot of sample 23005. The sensitivity corrected natural signal is depicted as an open square and the dashed line shows the equivalent dose. The response to a zero dose (recuperation) is shown as open circle. The recycling point is represented as an open inverted triangle. The inset displays a typical decay curve of natural CW-OSL (continuous-wave OSL signal) (full blue line) in comparison to a regenerated signal (full black line) induced by a beta dose approximately equal to the equivalent dose.

while the natural and regenerative decay curves are nearly indistinguishable from each other. This confirms that the OSL signal is dominated by the fast component. The average recuperation (response to a zero dose) for all measured aliquots (n = 443) is very low, averaging at 0.00 ± 0.02%. The recycling ratio was close to unity (1.00 ± 0.01) which confirms that the sensitivity change corrections during the SAR measurements were conducted accurately. The depletion ratio is likewise close to unity (0.98 ± 0.01) confirming that the extracted quartz is pure and no noticeable feldspar contamination is present. The recycling ratio, recuperation and depletion data for each sample are presented in Table S1.

The calculated D_es for the Kisiljevo LPS samples range from 1.47 ± 0.13 Gy (sample 23001) to 101.31 ± 4.88 Gy (sample 23016). The D_e values exhibit a generally increasing trend (within error limits) down to a depth of 600 cm cm (sample 23013). Here, a drop of 13 Gy is noticeable when compared to the overlying sample 23012 (550 cm depth). Below this depth, the samples continue to display increasing D_e values down to 800 cm (sample 23017) where a decrease of ~9 Gy is noticeable.

Wintle and Murray (2006) proposed that, for the fast component of the quartz OSL signal, as measured through the SAR protocol, the upper dose limit should be set at 2 × *D0*, corresponding to 86% saturation of the laboratory dose-response curve. Hence, to assess the proximity of the natural sensitivity-corrected luminescence signals to laboratory saturation for all quartz samples, we calculated the ratio between the natural sensitivity-corrected luminescence signal and the average maximum corrected luminescence signals induced by a dose of ~12,000 Gy. The maximum corrected luminescence signal was determined by constructing a laboratory DRC up to 12,000 Gy using sample 23019 (for details see Data in Brief). The calculated average ratios of the sensitivity-adjusted natural signal to the laboratory saturation level vary from 0.14 ± 0.02 (for sample 23001) to 0.49 ± 0.06 (for sample 23002), yielding a mean value of 0.36 ± 0.02. Based on this criterion, all calculated OSL ages were accepted for the Kisiljevo LPS (Fig. 6A).

As none of the quartz samples reached full laboratory saturation, we have conducted an additional saturation test according to Timar-Gabor and Wintle (2013), by adding large doses of 511 and 1022 Gy on top of the natural dose of sample 23019 (3 aliquots per dose). One aliquot per dose was rejected due to a depletion ration higher than 10%.

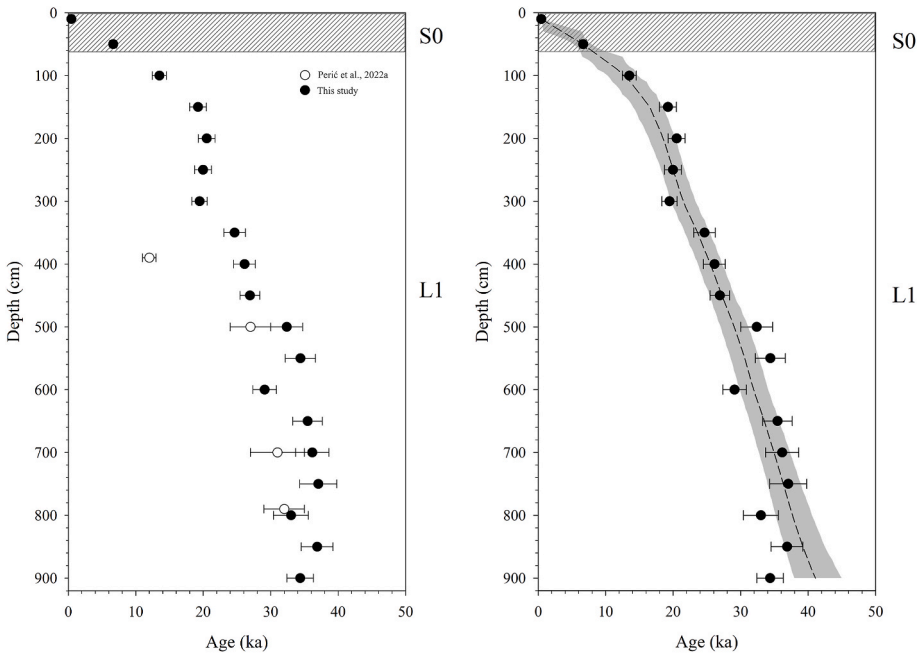

Fig. 6. A. OSL ages from the Kisiljevo LPS plotted against depth (black closed circles) and OSL ages from the initial study (opened white circles) presented in Perić et al. (2022a). B. Age-depth model for the Kisiljevo LPS. The black closed circles show the OSL ages. The grey shaded area represents the maximum and minimum age limits with a 95% certainty while the dashed line shows the mean age-depth model. The results were obtained using the rbacon age-depth modelling method (see text for details). The stratigraphic nomenclatures S0 and L1 are used following the stratigraphic model by Marković et al. (2015).

Subsequently, dose-response curves were generated up to ~11,000 Gy. Both DRCs exhibited incomplete saturation levels. The measured D_e values were 526 ± 16 Gy for the 511 Gy dose and 995 ± 40 Gy for the 1022 Gy dose. These results indicate doses approximately 11 ± 3% and 10 ± 4% lower than the anticipated doses of 593 Gy and 1104 Gy respectively. These findings suggest that the 63–90 μm quartz from Kisiljevo is able of accurately measuring (nearly within 10% deviation) a known dose within the high-dose range (for details see Data in Brief). This disagrees with the findings of Timar-Gabor and Wintle (2013), Timar-Gabor et al. (2015) and Perić et al. (2021) for Romanian and Serbian loess respectively. Here, it was concluded that quartz from this region cannot be used for measuring a known given dose in the high dose range and that most measurements overestimated the expected doses. However, it must be noted, that in the mentioned studies, the investigated quartz was mostly fine-grained (4–11 μm). Given the limitation and of the obtained data and scarcity of measurements, we do not necessarily imply that loess from this region is able to extend the current quartz OSL dating age limit. It is possible that the quartz characteristics are site or grain size specific and are not reproducible at other LPS in this region. Moreover, we recognize the probability that the measured doses might exceed the reliable range of measurement of natural doses in quartz OSL dating (Buylaert et al., 2007; Perić et al., 2019; Roberts, 2008). However, we do consider that these findings are sufficient to initiate more detailed investigations on the saturation behaviour for quartz from the Carpathian Basin, encompassing more sites and different grain sizes.

4.3. Age-depth model and dust flux estimates

The constructed rbacon age-depth model is shown in Fig. 6B. It is noticeable that all the luminescence ages overlap with the age model (within 95% of confidence). The rbacon age-depth model shows a considerable level of sensitivity to the alterations in luminescence age with depth which yielded a more exponential age-depth function. Moreover, the model suggests fluctuating MARs at least within the error limits of the method used.

The MARs for the Kisiljevo LPS are shown in Fig. 7 and range from 97 to 581 g/m^2/a, with a mean ($\bar{x}$) of 417 g/m^2/a and a median ($\tilde{x}$) of 421 g/m^2/a. During the investigated time period, three pronounced MAR peaks were observed: between 38 and 33 ka (MIS 3), between 32 and 30 ka (end of MIS 3), and between 21 and 19 ka (MIS 2) with mean MARs of 538, 559 and 516 g/m^2/a respectively. All through the observed time interval, the MARs display high variability. Absolute maximum values were reached during the end of MIS 3 (centred at 31 ka) with $\bar{x}$ = 581 g/m^2/a, while the lowest MARs were, expectedly, observed during MIS 1 (0.5–3 ka) with $\bar{x}$ = 97 g/m^2/a. For the MIS 3 period, the MAR values range from 329 to 581 g/m^2/a ($\bar{x}$ = 502 g/m^2/a, $\tilde{x}$ = 507 g/m^2/a).

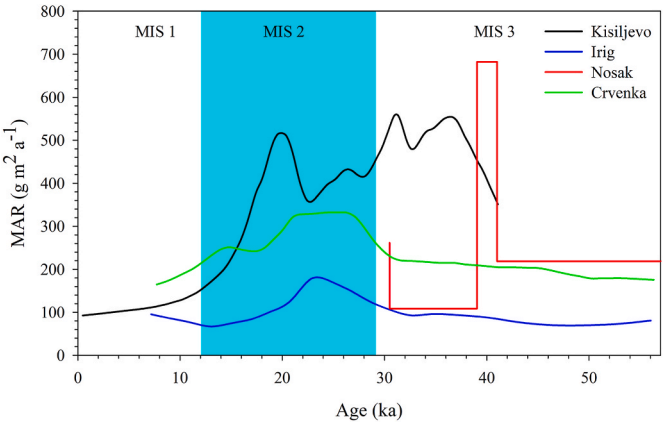

Fig. 7. Dust Mass Accumulation Rate (MAR) as a function of age for the Kisiljevo LPS. Also presented are the MARs for the Irig, Nosak and Crvenka LPS. The curves present the MARs according to the mean ages at a 95% confidence interval. For a more realistic representation the results were smoothed using the loess smoothing technique with tricube weighting and polynomial regression in the SigmaPlot software version 11.0 (sampling proportion = 0.100; polynomial degree = 1).

Although only the later part of MIS 3 is present at the site (41–29 ka), which is why we are not able to provide a complete picture of dust flux

for the period, the lowest MARs are observed during the middle stages of this phase (centred at 41 ka) with $\bar{x} = 348$ g/m^2/a, $\tilde{x} = 340$ g/m^2/a. There is an observable increasing trend towards the onset of MIS 2 (Fig. 7), where the maximum MAR value for MIS 3 is reached. During MIS 2, the MARs display a high level of fluctuation, with two distinct peaks: between 21 and 18 ka with a mean MAR value of 516 g/m^2/a. All through MIS 1, the MARs show a steady decrease towards present time.

The peak MARs for MIS 1 are witnessed at the onset of the phase with $\bar{x} = 153$ g/m^2/a, while the lowest values are seen between 2 and 0.5 ka ($\bar{x} = 97$ g/m^2/a).

5. Discussion

5.1. OSL chronology and age-depth model

The calculated quartz OSL ages for the Kisiljevo LPS are shown in Fig. 6A as a function of depth. It can be seen that the ages show a steady increase with depth, exhibit no large jumps or decreases and range from 0.46 ± 0.04 ka for sample 23001 (10 cm depth) to 37.05 ± 2.74 ka for sample 23016 (750 cm depth), suggesting that the profile deposited between the later stage of MIS 3 and MIS 1. The sole exception is sample 23013 (600 cm depth) where an age inversion, (outside of uncertainty) of ~5 ka was observed. This could potentially be an indicator for bioturbation at this depth, which resulted in post-depositional sediment mixing. From 600 cm depth, to the base of the profile, the OSL ages continue to increase down to a depth of 800 cm (sample 23017). Hereafter the ages display no significant increase, however, they still remain well within uncertainty limits. This could potentially be an indication of very high dust deposition activity during the middle and late stage of MIS 3, however, it can also suggest the possibility that the quartz from the Kisiljevo LPS reached the level of reliable measurement of natural doses. Indeed, there were several cases where, in spite of successfully performed dose recovery tests in high dose ranges, and the samples being well below the 2 × *D0* limit, the natural doses showed no increases, displayed scattering and age inversions for samples beyond 35 ka (>150 Gy). Such instances have been reported on a global scale, most notably in Romania (Constantin et al., 2014; Timar-Gabor et al., 2011, 2017), Serbia (Perić et al., 2019, 2022b), Germany (Zhang et al., 2023), and even for the Chinese Loess Plateau (e.g. Buylaert et al., 2007; Chapot et al., 2012; Lai, 2010; Perić et al., 2019; Wang et al., 2021). This could imply that the lifetime of a natural quartz OSL signal may be considerably shorter than the laboratory experiments suggest. Still, here we cannot confirm this assumption as it would require additional investigations on older samples from the Kisiljevo LPS, which, for this site is not possible (maximum depth at Kisiljevo LPS is 900 cm). Nevertheless, the three lowermost ages still show consistency (within uncertainty) and are well below 150 Gy, which is why we include them in the age model.

The rbacon generated age-depth model for the Kisiljevo LPS is presented in Fig. 6B. The mean ages show no jumps or reversals (within uncertainty), which suggests that no significant hiatuses or sedimentation breaks are present at the site. The L1 loess layer was dated between 41.4 ± 2.6 ka and 6.7 ± 0.5 ka, encompassing MIS 3, MIS 2 and MIS 1. Since the composition of the Kisiljevo LPS is fairly uniform, with no obvious MIS 3 soil development, it was not possible to establish expected ages for this site, based on correlation of loess-soil stratigraphic boundaries to the marine benthic oxygen isotope record (Lisiecki and Raymo, 2005). According to our ages, it is obvious that dust deposition at Kisiljevo started during the middle part of MIS 3 and continues to the present day. It is possible that a weak MIS 3 palaeosol is present at the site which is not detectable, however it is more likely that the continuous dust activity and deposition prevented the development of any significant soil layer during that period. Indeed, weakly developed paleo-soils are also very poorly visible on the nearby Nosak LPS (Marković et al., 2014) and Požarevac (Marković et al., 2021; Perić et al., 2021) profiles within the last glacial loess unit L1, indicating the dominance of dust input over pedogenetic processes. The age for the L1-S0 boundary was dated at 6.7 ± 0.5 ka, indicating that substantial loess accumulation was present well into the Holocene. Although there is a significant lack of detected and investigated LPS in north-eastern Serbia, which makes significant correlations not feasible, similar S0 ages were reported for numerous LPS in the Vojvodina region: Crvenka (7.7 ± 0.6 ka; Stevens et al., 2011), Veliki Surduk (7.4 ± 0.7 ka; Perić et al., 2019) Stari Slankamen (7.3 ± 0.4 ka; Murray et al., 2014) and Irig (7.1 ± 0.5 ka; Perić et al., 2022b) which are in good agreement with the ages for Kisiljevo.

5.2. Comparison to the previous chronology of the Kisiljevo LPS

Fig. 6A and Table 2 show the chronology proposed by Perić et al. (2022a) in comparison with the OSL ages from this study. Here, we have to highlight (as stated in section 4.1) that the sampling was not conducted at the same section of the profile. One of the reasons was that the original sampling surface became heavily eroded and weathered and the overhang which was present at the time of the primary field study collapsed.

This made sampling of the initial surface not possible. In addition, only two ages were taken at the same depth in both studies (700 and 500 cm), which is why we expect some degree of deviation between the two age sets. Nevertheless, to deem the initial ages reliable, this discrepancy should not exceed 10% for samples recovered at the same depth.

It can be seen that the ages at 800 cm depth (790 cm in Perić et al., 2022a) show an excellent correspondence in spite of the 10 cm sampling difference. The samples at 700 and 500 cm depth also display a good agreement (within uncertainty), albeit, in this case the ages presented in Perić et al. (2022a) display a slight underestimation in comparison to their counterparts from this study. Nevertheless, they are still well in the range of acceptable values.

However, the largest discrepancy was observed between the samples at 400 cm (390 cm in the original study). Here, the initial sample shows an underestimation of 11 ka (outside uncertainty) when compared to its corresponding sample from this study. Such a large deviation is not justifiable by a methodological variance nor the slightly different sampling depth. There are numerous causes that could explain the observed age deviation between the two samples, however, the two most likely reasons could be partial bleaching or post-depositional mixing. Although not likely, the sediment could have been unintentionally exposed to sunlight during the sampling which led to a partial resetting of the OSL signal, thus resulting in a lower age. One other possibility is post-depositional mixing due to bioturbation. There are clear signs of burrowing animal activities and distinct root channels on the sampling surface which could have mixed and disturbed this sediment layer. This would have largely affected the accuracy of the measurement procedure and subsequently resulted in a much younger age.

Currently, we are unable to determine the exact cause of the observed age underestimation. However, given that the OSL ages presented in this study show a steady increase with depth, display no large

Table 2
Summary of depth information, sample codes, OSL ages and total errors in ka for the Kisiljevo LPS from this study and the study by Perić et al. (2022a).

Sample (this study)	Depth (this study)	Age ka (this study)	Sample (Perić et al., 2022a)	Depth (Perić et al., 2022a)	Age ka (Perić et al., 2022a)
23009	400	26.1 ± 1.6	ZAT 2/0.395	390	12 ± 1
23011	500	32.4 ± 2.4	ZAT 1/0.23	500	27 ± 3
23015	700	36.2 ± 2.5	ZAT 1/0.41	700	31 ± 4
23017	800	34.4 ± 2.0	ZAT 1/0.47	790	32 ± 3

jumps or inversions and are stratigraphically consistent, we conclude that the uppermost age at the Kisiljevo LPS presented by Perić et al. (2022a) is ultimately erroneous and should be considered as unreliable.

5.3. MARs

The calculated MARs for the Kisiljevo LPS are shown in Fig. 7 and Table S2. It can be seen that the MAR values display a high level of oscillations during the investigated time period. While it is generally accepted that higher rates of dust accumulation arise during the cold glacial phases while lower rates occur during the warmer, interglacial stages (Kohfeld and Harrison, 2003; Stevens et al., 2011; Sun and An, 2005; Zhang et al., 1999, 2002), the MAR trend at Kisiljevo deviates from that model. Although, not the entirety of MIS 3 is represented at the site, which hampers a more complete dust flux interpretation, it can be seen that two distinct peaks in dustiness during this period occurred 38–33 ka and 32–30 ka where the MARs reach their maximum values (centred at 31 ka). As already stated, there are no available chronologies for LPS in north-eastern Serbia where MIS 2 and MIS 1 are represented. The closest investigated LPS in this region is Nosak (Perić et al., 2020), where the MIS 7-MIS 3 period was dated. When compared to the Kisiljevo LPS, it is noticeable that the MAR trend at Nosak during MIS 3, displays some comparable features. Also, at Nosak, there is a distinct MAR peak during MIS 3, with very high values (682 g/m^2/a), albeit occurring earlier in the phase than at Kisiljevo (42–36 ka). Here we consider the possibility that the high MIS 3 MARs could potentially be an artefact of dating uncertainties, however, given the fact that a similar trend is observed at another LPS in the vicinity (Nosak), it is more likely that this is a true representation of atmospheric dust activity for this region.

Conversely, the most investigated LPS in the Vojvodina region show a more consistent MAR trend during MIS 3. For instance, at the Irig (Perić et al., 2022b) and Crvenka LPS (Stevens et al., 2011), no pronounced MAR peaks are noticeable during MIS 3 (Fig. 7), instead a steady dust flux is observed throughout the phase. Such trend at Kisiljevo and Nosak, which differs from the ones observed at most LPS in Vojvodina, may be the result of site or region-specific factors. Increased transportation rates, improved trapping efficiency, elevated palaeowind intensity (Gavrilov et al., 2018), or the closer proximity of the Danube River could have played a role in the enhanced dust deposition during MIS 3.

The MAR trend during MIS 2 is more agreeable with the general dust deposition model. There is a clear peak during the middle part of the stage (22–17 ka) where the MARs reach their maximum values for this phase (centred at 19 ka) after which a constant decreasing trend towards the onset of the Holocene is observable. Such pattern is broadly consistent with most LPS in the Carpathian Basin. For example at Veliki Surduk LPS (Perić et al., 2019), MAR peaks were noted ~30–20 ka, centred on 25 ka and extending towards the Holocene (Perić et al., 2022b). In case of the Irig LPS the MAR peak was observed between 28 and 21 ka where a mean value of 164 g/m^2/a was recorded. A similar trend is notable at Crvenka LPS (Stevens et al., 2011), where increased dust deposition occurred ~28–19 ka. It is clear that peak dustiness at Kisiljevo transpired rather later in the phase than at other investigated LPS. This does not correspond with the increase of dust activity in Greenland (Ruth et al., 2007) nor the North Pacific (Hovan et al., 1989) which was observed ~26–23 ka. Moreover, the peak MARs at Kisiljevo during MIS 2 does not coincide with the Heinrich event 2 which is centred at ~24 ka (Hemming, 2004). During this period heightened atmospheric dust activity was recorded on an intercontinental scale, most notably: Greenland (Rasmussen et al., 2014), Western Europe (Stevens et al., 2020), and the Chinese Loess Plateau (Kang et al., 2015; Stevens et al., 2016). At present, there are no clear indications on the cause of this lag. However, several area specific factors could have caused a later increase of atmospheric dust activity at the Kisiljevo LPS, such as: the relative proximity of the Danube River as the main silt source, diverse geomorphological features of this area, more efficient trapping and/or palaeowind intensity (Perić et al., 2022b).

During MIS 1 the MARs display a decreasing tendency. The highest values are recorded at the start of the Holocene, steady declining towards the present. This is consistent with the majority of LPS in the Carpathian Basin (e.g. Fuchs et al., 2008; Murray et al., 2014; Perić et al., 2019) where atmospheric dust activity weakened with the onset of a warmer climate.

6. Conclusions

In conclusion, our updated, high-resolution OSL chronology for the Kisiljevo LPS in north-eastern Serbia has significantly enhanced our understanding of the paleoenvironmental dynamics in the region. The Kisiljevo LPS, initially thought to be a small, isolated loess "spot," was revealed through a detailed field survey to be part of a much larger loess plateau, extending over 2 km north-west and at least 0.5 km south of the investigated profile. Despite challenges in determining the true extent of the loess-covered area due to terrain transformation, the findings shed light on the broader geological context of the region. Comparison with the previous chronology by Perić et al. (2022a) highlights discrepancies, particularly at 400 cm depth, where a substantial age underestimation is observed. While differences in sampling depth and methodology may contribute to some variations, the magnitude of the deviation raises concerns about the reliability of the earlier chronology. The robustness of our new age-depth model and the continuous increase in ages with depth suggest that the earlier chronology might have underestimated the uppermost layer, possibly due to partial bleaching or post-depositional mixing. The age-depth model, constructed using Bayesian modelling, showcases a continuous sedimentation history from the later stages of MIS 3 to the present day. The calculated MARs exhibit intriguing patterns, with distinctive peaks during MIS 3 and the middle of MIS 2, deviating from typical dust deposition models. The peak dustiness during MIS 3 might be attributed to regional factors like increased transportation rates, enhanced trapping efficiency, or elevated palaeowind intensity. This study not only refines our understanding of the Kisiljevo LPS but also contributes valuable insights into the regional paleoenvironmental dynamics, emphasizing the need for careful consideration of local geological variations in reconstructing past climates from sediment archives. The MAR trends provide a basis for future investigations into the factors influencing dust deposition in north-eastern Serbia and offer a valuable reference for broader paleoclimatic interpretations in the Carpathian Basin.

Data availability

All data are available from the corresponding author upon reasonable request.

CRediT authorship contribution statement

Zoran M. Perić: Writing – review & editing, Writing – original draft, Visualization, Validation, Supervision, Software, Resources, Project administration, Methodology, Investigation, Funding acquisition, Formal analysis, Data curation, Conceptualization. **Cathal Ryan:** Writing – review & editing, Writing – original draft, Resources, Investigation, Data curation. **Helena Alexanderson:** Writing – original draft, Supervision, Methodology, Formal analysis, Data curation, Conceptualization. **Slobodan B. Marković:** Writing – review & editing, Writing – original draft, Supervision, Methodology, Investigation, Data curation.

Declaration of competing interest

The authors declare that they have no known competing financial interests or personal relationships that could have appeared to influence the work reported in this paper.

Acknowledgments

ZP is grateful for the support of the Royal Physiographic Society in Lund (grants no. 42788 and 43046) for supporting his research on the age of loess in the Carpathian Basin. This research was conducted within the Lu^2D^2 (The Lund Luminescence centre for Dating and Dosimetry) infrastructure.

Appendix A. Supplementary data

Supplementary data to this article can be found online at https://doi.org/10.1016/j.quaint.2024.06.006.

References

Albani, S., Mahowald, N.M., Winckler, G., Anderson, R.F., Bradtmiller, L.I., Delmonte, B., François, R., Goman, M., Heavens, N.G., Hesse, P.P., Hovan, S.A., Kang, S.G., Kohfeld, K.E., Lu, H., Maggi, V., Mason, J.A., Mayewski, P.A., McGee, D., Miao, X., Otto-Bliesner, B.L., Perry, A.T., Pourmand, A., Roberts, H.M., Rosenbloom, N., Stevens, T., Sun, J., 2015. Twelve thousand years of dust: the Holocene global dust cycle constrained by natural archives. Clim. Past 11, 869–903. https://doi.org/10.5194/CP-11-869-2015.

Antoine, P., Rousseau, D.D., Fuchs, M., Hatté, C., Gauthier, C., Marković, S.B., Jovanović, M., Gaudenyi, T., Moine, O., Rossignol, J., 2009. High-resolution record of the last climatic cycle in the southern Carpathian Basin (Surduk, Vojvodina, Serbia). Quat. Int. 198, 19–36. https://doi.org/10.1016/J.QUAINT.2008.12.008.

Blaauw, M., Christen, J.A., 2011. Flexible paleoclimate age-depth models using an autoregressive gamma process. Bayesian Anal 6, 457–474. https://doi.org/10.1214/11-BA618.

Bøtter-Jensen, L., Andersen, C.E., Duller, G.A.T., Murray, A.S., 2003. Developments in radiation, stimulation and observation facilities in luminescence measurements. Radiat. Meas. 37, 535–541. https://doi.org/10.1016/S1350-4487(03)00020-9.

Brennan, B.J., Lyons, R.G., Phillips, S.W., 1991. Attenuation of alpha particle track dose for spherical grains. Int. J. Radiat. Appl. Instrum. Part Nucl. Tracks Radiat. Meas. 18, 249–253. https://doi.org/10.1016/1359-0189(91)90119-3.

Buylaert, J.P., Vandenberghe, D., Murray, A.S., Huot, S., De Corte, F., Van den Haute, P., 2007. Luminescence dating of old (>70 ka) Chinese loess: a comparison of single-aliquot OSL and IRSL techniques. Quat. Geochronol. 2, 9–14. https://doi.org/10.1016/J.QUAGEO.2006.05.028.

Chapot, M.S., Roberts, H.M., Duller, G.A.T., Lai, Z.P., 2012. A comparison of natural- and laboratory-generated dose response curves for quartz optically stimulated luminescence signals from Chinese Loess. Radiat. Meas. 47, 1045–1052. https://doi.org/10.1016/j.radmeas.2012.09.001.

Constantin, D., Begy, R., Vasiliniuc, S., Panaiotu, C., Necula, C., Codrea, V., Timar-Gabor, A., 2014. High-resolution OSL dating of the Costineşti section (Dobrogea, SE Romania) using fine and coarse quartz. Quat. Int. 334–335, 20–29. https://doi.org/10.1016/J.QUAINT.2013.06.016.

Duller, G.A.T., 2015. The Analyst software package for luminescence data: overview and recent improvements. Anc. TL 33, 35–42.

Duller, G.A.T., 2003. Distinguishing quartz and feldspar in single grain luminescence measurements. Radiat. Meas. 37, 161–165. https://doi.org/10.1016/S1350-4487(02)00170-1.

Durcan, J.A., King, G.E., Duller, G.A.T., 2015. DRAC: dose rate and age calculator for trapped charge dating. Quat. Geochronol. 28, 54–61. https://doi.org/10.1016/j.quageo.2015.03.012.

Frechen, M., Oches, E.A., Kohfeld, K.E., 2003. Loess in Europe - mass accumulation rates during the last glacial period. Quat. Sci. Rev. 22, 1835–1857. https://doi.org/10.1016/S0277-3791(03)00183-5.

Fuchs, M., Rousseau, D.D., Antoine, P., Hatté, C., Gauthier, C., Marković, S., Zoeller, L., 2008. Chronology of the last climatic cycle (upper Pleistocene) of the Surduk loess sequence, Vojvodina, Serbia. Boreas 37, 66–73. https://doi.org/10.1111/J.1502-3885.2007.00012.X.

Gavrilov, M.B., Marković, S.B., Schaetzl, R.J., Tošić, I., Zeeden, C., Obreht, I., Sipos, G., Ruman, A., Putniković, S., Emunds, K., Perić, Z., Hambach, U., Lehmkuhl, F., 2018. Prevailing surface winds in Northern Serbia in the recent and past time periods; modern- and past dust deposition. Aeolian Res 31, 117–129. https://doi.org/10.1016/J.AEOLIA.2017.07.008.

Guérin, G., Mercier, N., Adamiec, G., 2011. Dose-rate conversion factors: update. Anc. TL 29, 5–8.

Guérin, G., Mercier, N., Nathan, R., Adamiec, G., Lefrais, Y., 2012. On the use of the infinite matrix assumption and associated concepts: a critical review. Radiat. Meas., Proceedings of the 13th International Conference on Luminescence and Electron Spin Resonance Dating 47, 778–785. https://doi.org/10.1016/j.radmeas.2012.04.004, 10–14 July, 2011, Toruń, Poland.

Hansen, V., Murray, A., Buylaert, J.-P., Yeo, E.-Y., Thomsen, K., 2015. A new irradiated quartz for beta source calibration. Radiat. Meas. 81, 123–127. https://doi.org/10.1016/j.radmeas.2015.02.017.

Hemming, S.R., 2004. Heinrich events: massive late Pleistocene detritus layers of the North Atlantic and their global climate imprint. Rev. Geophys. 42 https://doi.org/10.1029/2003RG000128.

Hovan, S.A., Rea, D.K., Pisias, N.G., Shackleton, N.J., 1989. A direct link between the China loess and marine δ18O records: aeolian flux to the north Pacific. Nature 340, 296–298.

Kang, S., Roberts, H.M., Wang, X., An, Z., Wang, M., 2015. Mass accumulation rate changes in Chinese loess during MIS 2, and asynchrony with records from Greenland ice cores and North Pacific Ocean sediments during the Last Glacial Maximum. Aeolian Res 19, 251–258. https://doi.org/10.1016/J.AEOLIA.2015.05.005.

Kohfeld, K.E., Harrison, S.P., 2003. Glacial-interglacial changes in dust deposition on the Chinese Loess Plateau. Quat. Sci. Rev. 22, 1859–1878. https://doi.org/10.1016/S0277-3791(03)00166-5.

Kohfeld, K.E., Harrison, S.P., 2001. DIRTMAP: the geological record of dust. Earth Sci. Rev. 54, 81–114. https://doi.org/10.1016/S0012-8252(01)00042-3.

Kolb, T., Tudyka, K., Kadereit, A., Lomax, J., Poręba, G., Zander, A., Zipf, L., Fuchs, M., 2022. The μDose system: determination of environmental dose rates by combined alpha and beta counting – performance tests and practical experiences. Geochronology 4, 1–31. https://doi.org/10.5194/gchron-4-1-2022.

Lai, Z.P., 2010. Chronology and the upper dating limit for loess samples from Luochuan section in the Chinese Loess Plateau using quartz OSL SAR protocol. J. Asian Earth Sci. 37, 176–185. https://doi.org/10.1016/J.JSEAES.2009.08.003.

Lehmkuhl, F., Bösken, J., Hošek, J., Sprafke, T., Marković, S.B., Obreht, I., Hambach, U., Sümegi, P., Thiemann, A., Steffens, S., Lindner, H., Veres, D., Zeeden, C., 2018. Loess distribution and related quaternary sediments in the Carpathian Basin. J. Maps 14, 661–670. https://doi.org/10.1080/17445647.2018.1526720.

Lisiecki, L.E., Raymo, M.E., 2005. A Pliocene-Pleistocene stack of 57 globally distributed benthic δ18O records. Paleoceanography 20. https://doi.org/10.1029/2004PA001071.

Marković, S.B., Korać, M., Mrdić, N., Buylaert, J.P., Thiel, C., McLaren, S.J., Stevens, T., Tomić, N., Petić, N., Jovanović, M., Vasiljević, D.A., Sümegi, P., Gavrilov, M.B., Obreht, I., 2014. Palaeoenvironment and geoconservation of mammoths from the Nosak loess-palaeosol sequence (Drmno, northeastern Serbia): initial results and perspectives. Quat. Int. 334–335, 30–39. https://doi.org/10.1016/j.quaint.2013.05.047.

Marković, S.B., Oches, E.A., Perić, Z.M., Gaudenyi, T., Jovanović, M., Sipos, G., Thiel, C., Buylaert, J.-P., Savić, S., Mccoy, W.D., Radaković, M.G., Marković, R.S., Gavrilov, M. B., 2021. The Požarevac loess-paleosol sequence: a record of increased aridity in the south-eastern margin of the Carpathian Basin during the last 350 ka. J. Quat. Sci. 1436–1447. https://doi.org/10.1002/jqs.3327.

Marković, S.B., Stevens, T., Kukla, G.J., Hambach, U., Fitzsimmons, K.E., Gibbard, P., Buggle, B., Zech, M., Guo, Z., Hao, Q., Wu, H., O'Hara Dhand, K., Smalley, I.J., Újvári, G., Sümegi, P., Timar-Gabor, A., Veres, D., Sirocko, F., Vasiljević, D.A., Jary, Z., Svensson, A., Jović, V., Lehmkuhl, F., Kovács, J., Svirčev, Z., 2015. Danube loess stratigraphy — towards a pan-European loess stratigraphic model. Earth Sci. Rev. 148, 228–258. https://doi.org/10.1016/J.EARSCIREV.2015.06.005.

Murray, A.S., Schmidt, E.D., Stevens, T., Buylaert, J.P., Marković, S.B., Tsukamoto, S., Frechen, M., 2014. Dating Middle Pleistocene loess from Stari Slankamen (Vojvodina, Serbia) — limitations imposed by the saturation behaviour of an elevated temperature IRSL signal. Catena 117, 34–42. https://doi.org/10.1016/J.CATENA.2013.06.029.

Murray, A.S., Wintle, A.G., 2003. The single aliquot regenerative dose protocol: potential for improvements in reliability. Radiat. Meas., Proceedings of the 10th international Conference on Luminescence and Electron-Spin Resonance Dating (LED 2002) 37, 377–381. https://doi.org/10.1016/S1350-4487(03)00053-2.

Murray, A.S., Wintle, A.G., 2000. Luminescence dating of quartz using an improved single-aliquot regenerative-dose protocol. Radiat. Meas. 32, 57–73. https://doi.org/10.1016/S1350-4487(99)00253-X.

Perić, Z., Lagerbäck Adolphi, E., Stevens, T., Újvári, G., Zeeden, C., Buylaert, J.P., Marković, S.B., Hambach, U., Fischer, P., Schmidt, C., Schulte, P., Huayu, L., Shuangwen, Y., Lehmkuhl, F., Obreht, I., Veres, D., Thiel, C., Frechen, M., Jain, M., Vött, A., Zöller, L., Gavrilov, M.B., 2019. Quartz OSL dating of late quaternary Chinese and Serbian loess: a cross Eurasian comparison of dust mass accumulation rates. Quat. Int. 502, 30–44. https://doi.org/10.1016/J.QUAINT.2018.01.010.

Perić, Z.M., Marković, S.B., Avram, A., Timar-Gabor, A., Zeeden, C., Nett, J.J., Fischer, P., Fitzsimmons, K.E., Gavrilov, M.B., 2022a. Initial quartz OSL and dust mass accumulation rate investigation of the Kisiljevo loess sequence in north-eastern Serbia. Quat. Int. 620, 13–23. https://doi.org/10.1016/J.QUAINT.2020.10.040.

Perić, Z.M., Marković, S.B., Filyó, D., Thiel, C., Murray, A.S., Gavrilov, M.B., Nett, J.J., Sipos, G., 2021. Quartz OSL and polymineral post IR–IRSL dating of the Požarevac loess–palaeosol sequence in north–eastern Serbia. Quat. Geochronol. 66, 101216 https://doi.org/10.1016/J.QUAGEO.2021.101216.

Perić, Z.M., Marković, S.B., Sipos, G., Gavrilov, M.B., Thiel, C., Zeeden, C., Murray, A.S., 2020. A post-IR IRSL chronology and dust mass accumulation rates of the Nosak loess-palaeosol sequence in northeastern Serbia. Boreas 49, 841–857. https://doi.org/10.1111/bor.12459.

Perić, Z.M., Stevens, T., Obreht, I., Hambach, U., Lehmkuhl, F., Marković, S.B., 2022b. Detailed luminescence dating of dust mass accumulation rates over the last two glacial-interglacial cycles from the Irig loess-palaeosol sequence, Carpathian Basin. Global Planet. Change 215, 103895. https://doi.org/10.1016/j.gloplacha.2022.103895.

Prescott, J.R., Hutton, J.T., 1994. Cosmic ray contributions to dose rates for luminescence and ESR dating: large depths and long-term time variations. Radiat. Meas. 23, 497–500. https://doi.org/10.1016/1350-4487(94)90086-8.

Rasmussen, S.O., Bigler, M., Blockley, S.P., Blunier, T., Buchardt, S.L., Clausen, H.B., Cvijanovic, I., Dahl-Jensen, D., Johnsen, S.J., Fischer, H., Gkinis, V., Guillevic, M., Hoek, W.Z., Lowe, J.J., Pedro, J.B., Popp, T., Seierstad, I.K., Steffensen, J.P., Svensson, A.M., Vallelonga, P., Vinther, B.M., Walker, M.J.C., Wheatley, J.J., Winstrup, M., 2014. A stratigraphic framework for abrupt climatic changes during

the Last Glacial period based on three synchronized Greenland ice-core records: refining and extending the INTIMATE event stratigraphy. Quat. Sci. Rev. 106, 14–28. https://doi.org/10.1016/J.QUASCIREV.2014.09.007.

Roberts, H.M., 2008. The development and application of luminescence dating to loess deposits: a perspective on the past, present and future. Boreas 37, 483–507. https://doi.org/10.1111/J.1502-3885.2008.00057.X.

Ruth, U., Bigler, M., Röthlisberger, R., Siggaard-Andersen, M., Kipfstuhl, S., Goto-Azuma, K., Hansson, M.E., Johnsen, S.J., Lu, H., Steffensen, J.P., 2007. Ice core evidence for a very tight link between North Atlantic and east Asian glacial climate. Geophys. Res. Lett. 34.

Schmidt, E.D., Machalett, B., Marković, S.B., Tsukamoto, S., Frechen, M., 2010. Luminescence chronology of the upper part of the Stari Slankamen loess sequence (Vojvodina, Serbia). Quat. Geochronol. 5, 137–142. https://doi.org/10.1016/J.QUAGEO.2009.09.006.

Stevens, T., Buylaert, J.P., Lu, H., Thiel, C., Murray, A., Frechen, M., Yi, S., Zeng, L., 2016. Mass accumulation rate and monsoon records from Xifeng, Chinese Loess Plateau, based on a luminescence age model. J. Quat. Sci. 31, 391–405. https://doi.org/10.1002/JQS.2848.

Stevens, T., Marković, S.B., Zech, M., Hambach, U., Sümegi, P., 2011. Dust deposition and climate in the Carpathian Basin over an independently dated last glacial-interglacial cycle. Quat. Sci. Rev. 30, 662–681. https://doi.org/10.1016/j.quascirev.2010.12.011.

Stevens, T., Sechi, D., Bradák, B., Orbe, R., Baykal, Y., Cossu, G., Tziavaras, C., Andreucci, S., Pascucci, V., 2020. Abrupt last glacial dust fall over southeast England associated with dynamics of the British-Irish ice sheet. Quat. Sci. Rev. 250, 106641 https://doi.org/10.1016/J.QUASCIREV.2020.106641.

Sun, Y., An, Z., 2005. Late Pliocene-Pleistocene changes in mass accumulation rates of eolian deposits on the central Chinese Loess Plateau. J. Geophys. Res. 110, D23101 https://doi.org/10.1029/2005JD006064.

Timar-Gabor, A., Buylaert, J.-P., Guralnik, B., Trandafir-Antohi, O., Constantin, D., Anechitei-Deacu, V., Jain, M., Murray, A.S., Porat, N., Hao, Q., Wintle, A.G., 2017. On the importance of grain size in luminescence dating using quartz. Proceedings of the 18th International Conference on Solid State Dosimetry (SSD18). Radiat. Meas., Munich, Germany, pp. 464–471. https://doi.org/10.1016/j.radmeas.2017.01.009, 3 – 8 July 2016 106.

Timar-Gabor, A., Constantin, D., Buylaert, J.P., Jain, M., Murray, A.S., Wintle, A.G., 2015. Fundamental investigations of natural and laboratory generated SAR dose response curves for quartz OSL in the high dose range. In: Radiat. Meas., 14th International Conference on Luminescence and Electron Spin Resonance Dating, 7–11 July, 2014, Montréal, Canada, pp. 150–156. https://doi.org/10.1016/j.radmeas.2015.01.013, 81.

Timar-Gabor, A., Vandenberghe, D.A.G., Vasiliniuc, S., Panaoitu, C.E., Panaiotu, C.G., Dimofte, D., Cosma, C., 2011. Optical dating of Romanian loess: a comparison between silt-sized and sand-sized quartz. Quat. Int., The Second Loessfest 240 (2009), 62–70. https://doi.org/10.1016/j.quaint.2010.10.007.

Timar-Gabor, A., Wintle, A.G., 2013. On natural and laboratory generated dose response curves for quartz of different grain sizes from Romanian loess. Quat. Geochronol. 18, 34–40. https://doi.org/10.1016/j.quageo.2013.08.001.

Tudyka, K., Koruszowic, M., Osadnik, R., Adamiec, G., Moska, P., Szymak, A., Bluszcz, A., Zhang, J., Kolb, T., Poręba, G., 2023. µRate: an online dose rate calculator for trapped charge dating. Archaeometry 65, 423–443. https://doi.org/10.1111/arcm.12828.

Újvári, G., Kovács, J., Varga, G., Raucsik, B., Marković, S.B., 2010. Dust flux estimates for the Last Glacial Period in East Central Europe based on terrestrial records of loess deposits: a review. Quat. Sci. Rev. 29, 3157–3166. https://doi.org/10.1016/J.QUASCIREV.2010.07.005.

Wang, X., Peng, J., Adamiec, G., 2021. Extending the age limit of quartz OSL dating of Chinese loess using a new multiple-aliquot regenerative-dose (MAR) protocol with carefully selected preheat conditions. Quat. Geochronol. 62 https://doi.org/10.1016/j.quageo.2020.101144.

Wintle, A.G., 1993. Luminescence dating of aeolian sands: an overview. Geol. Soc. Lond. Spec. Publ. 72, 49–58. https://doi.org/10.1144/GSL.SP.1993.072.01.06.

Wintle, A.G., Murray, A.S., 2006. A review of quartz optically stimulated luminescence characteristics and their relevance in single-aliquot regeneration dating protocols. Radiat. Meas. 41, 369–391. https://doi.org/10.1016/J.RADMEAS.2005.11.001.

Zhang, J., Zolitschka, B., Hogrefe, I., Tsukamoto, S., Binot, F., Frechen, M., 2023. High-resolution Luminescence-Dated Sediment Record for the Last Two Glacial-Interglacial Cycles from Rodderberg, Germany.

Zhang, X.Y., Arimoto, R., An, Z.S., 1999. Glacial and interglacial patterns for Asian dust transport. Quat. Sci. Rev. 18, 811–819.

Zhang, X.Y., Lu, H.Y., Arimoto, R., Gong, S., 2002. Atmospheric dust loadings and their relationship to rapid oscillations of the Asian winter monsoon climate: two 250-kyr loess records. Earth Planet Sci. Lett. 202, 637–643.